ARTICLE TYPE www.rsc.org/xxxxxx | XXXXXXXX

Structure of a uranyl peroxo complex in aqueous solution from first-principles molecular dynamics simulations.†

Michael Bühl,*[a] Nicolas Sieffert,[b] and Georges Wipff[c]

Received (in XXX, XXX) Xth XXXXXXXXX 200X, Accepted Xth XXXXXXXXX 200X ***Revised version 21 October 2013***
First published on the web Xth XXXXXXXXX 200X
DOI: 10.1039/b000000x

Static ab initio and density-functional computations, as well as Car-Parrinello molecular dynamics simulations in aqueous solution are reported for $[UO_2(OH)(\kappa^2\text{-}O_2)(H_2O)_2]^-$ and $[UO_2(OH)_2(\kappa^1\text{-}O_2H)(H_2O)]^-$. Whereas the κ^1-hydroperoxo isomer is found more stable than the κ^2-peroxo form in the gas phase, the order of stability is reversed in explicit bulk solution. Based on free energies from thermodynamic integration (BLYP functional), the peroxo form is favoured by ca. 32 kJ/mol in water. This stabilisation is discussed in terms of the hydration shells about the individual ligands and dipole moments of the complexes in water, and highlights the importance of explicit solute-solvent interactions and bulk solvation for the speciation of uranyl(VI) compounds.

1 Introduction

The high affinity between the uranyl(VI) ion and peroxide can affect nuclear waste management, because hydrogen peroxide is generated from water through α-radiolysis.[1] Not only can uranyl peroxides take part in the complex speciation equilibria whenever α-emitters and water are present, such peroxides have also been implicated in the enhanced corrosion of spent nuclear fuel by seawater.[2] Uranyl-peroxo complexes are well known in the solid, e.g. in form of the studtite minerals such as $[UO_2(O_2)](H_2O)_4$,[3,4] or giant cluster compounds up to $[UO_2(OH)(O_2)]_{60}^{60-}$.[5] The latter have attracted much interest of late, contributing to the unabated renaissance of uranyl chemistry.[6]

Uranyl peroxides are insoluble in acidic media, but soluble in aqueous alkaline solutions.[7] The speciation of ternary $UO_2^{2+}/OH^-/H_2O_2$[8] and $UO_2^{2+}/H_2O_2/CO_3^{2-}$ systems[9] in aqueous solution has recently been studied using potentiometric and spectrophotometric techniques, the former system more recently also through quenching of laser-induced fluorescence,[10] the latter through Raman spectroscopy.[11] In keeping with the tendency of hydroxo and peroxo complexes to aggregate and condensate, not only mononuclear, but also di- and trinuclear species have been characterised spectrophotometrically as a function of pH.[8] While the overall composition of the complexes (including the protonation state) can be deduced this way, their precise structure cannot. As Grenthe and coworkers note, "it is not possible to distinguish between the stochiometry of $[(UO_2)_p(OH)_q(HO_2)_r]^{2p-q-r}$ and $[(UO_2)_p(OH)_{q-r}(O_2)_r]^{2p-q-r}$",[8] [i.e. whether the complexes contain peroxo (O_2^{2-}) or hydroperoxo ligands (HO_2^-), see Chart 1], and they further state that "additional chemical information, for instance from the coordination geometry in solid state structures, has to be used to do this". We now propose to use information from quantum-chemical computations for this purpose.[12]

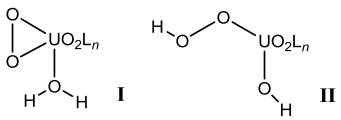

Chart 1: Possible tautomeric structures for uranyl peroxo species in aqueous alkaine solution.

Such computations have a long history and are now well established for actinide compounds in general, and uranyl complexes in particular.[13] Because of their relatively favourable computational expense, methods rooted in density functional theory (DFT) are becoming increasingly popular. For uranyl-peroxo complexes, recent computational studies have focused mainly on hydrated binary complexes of the type $[UO_2(O_2)_r(H_2O)_x]^{2-2r}$, calling special attention to their structural and vibrational[14] or their bonding properties.[15] Studtite has also been investigated through periodic DFT calculations.[16] All of these studies have employed static geometry optimisations and, for the molecular species, vibrational frequency calculations, with solvation effects included implicitly through polarisable continuum models (PCMs). Potential shortcomings of such PCMs for polar protic solvents such as water are well recognised, and specific interactions with the solvent (hydrogen bonds) can be included by considering microsolvated clusters containing few explicit water molecules.[17]

To go beyond the static picture, we have established the use of Car-Parrinello molecular dynamics (CPMD) simulations with explicit inclusion of the solvent to model a number of uranyl complexes in aqueous and non-aqueous solutions.[18,19,20] Using this method, together with a special numerical technique (pointwise thermodynamic integration, PTI), several thermodynamic and kinetic parameters of uranyl hydrate,

$[UO_2(H_2O)_5]^{2+}$, have been reproduced with an accuracy of ca. ±10 kJ/mol. We now apply this approach to a prototypical uranyl peroxo complex, calling special attention to the tautomeric equilibrium of Chart 1. As it turns out, gas-phase and PCM single-point calculations predict a tautomer corresponding to **II** to be the most stable, wheras optimisations in a continuum and CPMD simulations in an explicit water box favor the expected peroxo form **I**.

2 Computational details

The same methods and basis sets as in our previous studies of uranyl hydroxides and oxalates[18f-h] were employed (see Supporting Information, SI, for details and references). CPMD[21] / BLYP[22] simulations were performed in the NVT ensemble using a single Nosé-Hoover thermostat set to 320 K, a norm-conserving pseudopotential on U,[23] and a plane-wave cutoff of 80 Ry (100 Ry in selected cases). The slighly elevated temperature was chosen to keep the systems liquid-like and enhance sampling. Cubic supercells were used with a lattice contant of 13 Å, which contained uranyl, one peroxo moiety (O_2), one OH^- and a total of 59 water molecules. The mirror images are well separated and cannot react with each other, e.g. via condensation. The BLYP functional was chosen because it performs better than most other standard GGAs for describing the properties of liquid water.[24] Using the same setup selected conformers were also optimised in the gas phase, and the most stable were reoptimised with a larger lattice constant of 15 Å (denoted CP-opt). These computations were performed with the CPMD program.[25]

Because the simulations were performed at constant volume, Helmholtz rather than Gibbs free energies are obtained, but in condensed phase the difference between both is very small. No further dissection of the free energies into enthalpic and entropic contributions (which would require, in principle, simulations at different temperatures) was attempted, but for the tautomeric equilibria that are investigated, entropy effects are expected to be small.

Nonperiodic geometry optimisations were performed at BLYP, and B3LYP[26] levels, employing the small-core Stuttgart-Dresden relativistic ECP together with its valence basis set on U[27] (from which the most diffuse s-,p-,d-, and f-functions were omitted, affording a [7s6p5d3f] contraction),[28] standard 6-311G+(d,p) basis[29] for all other elements, and an ultrafine integration grid (99 radial shells with 590 angular points per shell), denoted SDD. The minimum character of each stationary point was verified by computation of the harmonic vibrational frequencies, which were all real. Refined single-point energies were evaluated using the B3LYP-optimized geometries,[30] the same SDD ECP and valence basis on U (augmented with a g-function with exponent 0.5), aug-cc-pVTZ basis[31] elsewhere (denoted SDDD+), and a variety of DFT and ab initio methods, namely, B3LYP, M06,[32] MP2, and CCSD(T). Selected single-point calculations employed the polarisable continuum model (PCM) in its integral equation formalism according to Tomasi and coworkers[33] (employing the UFF radii for all atoms and the parameters of water). These computations were performed with the Gaussian suite of programs,[34] except for the MP2 and CCSD(T) single points, which were obtained with NWChem.[35] Finally, empirical dispersion corrections were evaluated for B3LYP structures using the recent scheme by Grimme and coworkers (denoted B3LYP-D3).[36]

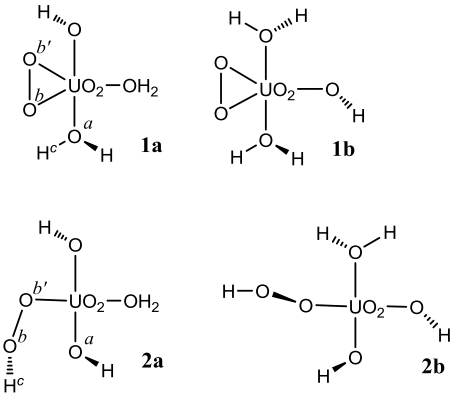

Chart 2: Mono-anionic uranyl-peroxo complexes considered this study, including labeling of selected O atoms.

3 Results and discussion

3.1 Static calculations

Rather than the neutral peroxo complex $[UO_2(O_2)(H_2O)_3]$ that had been previously studied using computational methods,[14,15] we chose anionic $[UO_2(OH)(O_2)(H_2O)_2]^-$ as a target, because this corresponds to the protonation state deduced experimentally by Grenthe and coworkers.[8] Some initial exploratory optimisations were performed in the gas phase at the CP-opt/BLYP level. With subsequent MD studies in mind, where aquo and hydroxo ligands can usually rotate rather freely, no exhaustive searches of the conformational space of these ligands were undertaken. For the peroxo tautomers **I**, the isomer with O_2 and OH ligand *cis* to each other (**1a**, Chart 2) is more stable than the corresponding *trans* form (**1b**) by 14.6 kJ/mol. Similarly, for the hydroperoxo tautomer **II**, the form with the two OH ligands *trans* (**2a**) is more stable than the corresponding *cis* isomer (**2b**, where the OOH moiety has also undergone a rotation out of the equatorial uranyl plane) by 5.8 kJ/mol. Because they can be interconverted via a simple proton transfer from O^a to O^b (see labeling in Chart 2), **1a** and **2a** were taken as starting and end point in constrained CPMD simulations in water (see section 3.2 below) and considered as representative for the tautomers **I** and **II**, respectively.

At the crude CP-opt/BLYP level, **2a** is 16.9 kJ/mol lower in energy than **1a**, a somewhat unexpected result, as side-on κ^2-O_2 complexes are rather common and have also been observed in uranyl peroxo complexes in the solid (as bridging units, though).[3] When refined with a higher plane-wave cutoff (corresponding to a bigger basis set), this energy difference is roughly halved (see Table 1). Structures and energies of these two tautomers were subsequently refined at a variety of DFT and ab initio wavefunction methods. At almost all levels included in Table 1, this energetic sequence is confirmed. At

the CCSD(T) level, the "gold standard" in quantum chemistry,[37] **2a** is more stable than **1a** by 32.9 kJ/mol.

Table 1. Relative energies of **2a** relative to **1a** (in kJ/mol) at selected levels of theory.[a]

Level	ΔE_{rel}	Level	ΔE_{rel}
BLYP/CP-opt[b]	-16.9	BLYP/SDD+	1.0
BLYP/CP-opt100[b,c]	-8.1	B3LYP/SDD+	-17.9
BLYP/SDD[b]	2.3	M06/SDD+	-21.1
B3LYP/SDD[b]	-18.3	HF/SDD+	-82.8
B3LYP/SDD-D3[d]	-16.9	MP2/SDD+	-14.0
B3LYP/SDD ΔG[e]	-19.2	CCSD/SDD+	-49.4
B3LYP/SDD/PCM[b,f]	4.2	CCSD(T)/SDD+	-32.9

[a]B3LYP/SDD+ geometries employed unless stated otherwise. [b]Fully optimised at the given level. [c]Optimised with a plane-wave cutoff of 100 Ry. [d]B3LYP/SDD geometries employed. [e]Free energies at standard pressure and 298.15 K. [f]Fully optimised; -33.1 kJ/mol if evaluated as single-point energy for gas-phase structures.

While dispersion and thermodynamic corrections are indicated to be small (compare B3LYP/SDD, B3LYP/SDD-D3 and B3LYP/SDD ΔG values in Table 1), a simple continuum solvation model predicts a notable stabilisation of **1a** in solution to the point that it becomes slightly favored over **2a** (compare B3LYP/SDD and B3LYP/SDD/PCM values). The stabilisation of **1a** is only apparent after optimisation in the continuum, not from PCM single points on gas phase geometries, where **2a** actually appears to be even more favoured than in the gas phase (see footnote [f] in Table 1).

The BLYP/SDD and BLYP/SDD+ energies stand out, because at these levels, both isomers are essentially isoenergetic in the gas phase. At the BLYP/CP-opt level, the hydroperoxo species **2a** is again noticeably lower in energy. The discrepancy between these levels, which must be due to the different pseudopotenatials, basis sets and isolated vs. periodic set-ups employed, is somewhat larger than unsually found (ca. 9 kJ/mol in this case with the largest basis sets, i.e. CP-opt100 vs. SDD+). We note that, somewhat fortuitously, the results with the lower BLYP/CP-opt level agree well with those of the more sophisticated functionals B3LYP and M06, the latter of which has been recommended for actinide complexes.[38]

Another noteworthy result in Table 1 is the apparent discrepancy between MP2, CCSD and CCSD(T) results. While MP2 and CCSD(T) data tend to be rather similar for "well-behaved" systems such as uranyl hydrate,[38,39] similarly pronounced oscillations have been observed for the relative stability of *cis*- and *trans*-uranyl complexes.[37,40] For an appraisal of the BLYP results in relation to the other DFT and the CCSD(T) data see below.

In order to estimate the effect of explicit solvation on these relative energies, we have optimised microsolvated clusters containing one additional water molecule in the second hydration shell. A few initial placements of this additional water were trialled for optimisation (though again no exhaustive search was undertaken). The resulting, most stable minima of each **1a**·H_2O and **2a**·H_2O are depicted in Figure 1. In both cases, a similar binding mode of the extra water molecule is realised, where it donates a H-bond either to O^a or O^b, the other OH bond aligning with a terminal U=O moiety. At the B3LYP/SDD level, the hydroperoxo isomer **2a**·H_2O is still preferred, but the energetic discrimination is essentially halved, from -18.3 kJ/mol (Table 1) to -8.9 kJ/mol. Again, optimisation in the continuum stabilises **1a**·H_2O, making it more stable than **2a**·H_2O by 9.1 kJ/mol at that level (see Figure S1 in the ESI for a plot of the optimised structures).

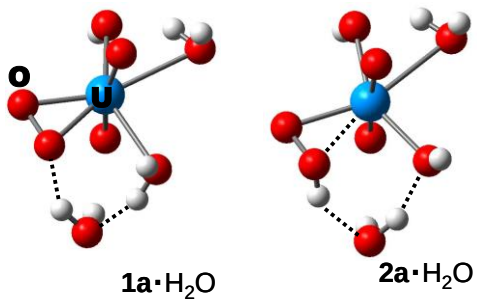

Figure 1: Microsolvated clusters of **1a** and **2a** (B3LYP/SDD optimised).

A similar result is obtained at the BLYP/SDD level, where pristine **1a**·H_2O (instead of being nearly isoenergetic with **2a**·H_2O) is now favoured by 6.6 kJ/mol. Evidently, including explicit water molecules can have a noticeble effect on the relative stabilies. Ultimately, more and more water molecules would have to be added, with a subsequent search for the global minima in each case, to converge these results. Because the statistical significance of each minimum is expected to decrease with increasing water coverage, we have adopted a fully dynamical description of the bulk solution, the results of which will be discussed in the following section.

3.2 CPMD simulations

When an unconstrained BLYP/CPMD simulation of **1a** was launched in the gas phase starting from the CP-opt minimum, both water molecules detached immediately, affording $[UO_2(OH)(\kappa^2\text{-}O_2)]^-\cdot 2H_2O$ with reduced coordination number about uranyl and two water molecules in the second hydration sphere. As frequently observed in these gas-phase simulations, the uranyl-water interaction appears to be too weak to keep the water coordinated to the metal, and microsolvated complexes with intermolecular H-bonds are preferred. This finding is presumably related to the inherent underestimation of metal-ligand binding energies in transition-metal hydrates with such simple gradient-corrected density functionals.[41]

A system containing **1a** in a periodic water box was then prepared starting from an equilibrated snapshot of a previous anionic system, namely $[UO_2(OH)_5]^{3-}$.[37] After replacing the uranyl hydroxide with the CP-opt structure of **1a**, the system was propagated freely (i.e. without constraints) in the NVT ensemble for 4 ps. The water ligand adjacent to the peroxide

dissociated quickly into the solution, to be replaced by another one from the bulk within the first 2 ps, restoring five-coordination about uranyl. No further spontaneous ligand dissociations were observed in this or in any of the subsequent free or constrained MD simulations in water. The structure of aqueous **1a** will be discussed in more detail at the end of this section.

From the last point of this simulation of **1a**, a starting point for aqueous **2a** was generated by manually opening up the U-O-O angle of the κ^2-UO_2 ring and moving a H atom from the adjacent water ligand to the "dangling" O atom of the resulting U-O-O moiety. Apart from a ca. 180° rotation of the hydroperoxo ligand about the U-$O^{b'}$ axis within the first 1.5 ps (passing through transient structures with *syn*-periplanar O=U-O-O units as in **2b**), **2a** was stable in an unconstrained MD simulation over 4 ps in total.

To probe whether a κ^1-U-O-O arrangement (with a formal negative charge on the dangling O atom) could be stable in water, an instantaneous snapshot from the latter trajectory with *syn*-periplanar O=U-O-O unit was chosen and the H atom manually moved from the hydroperoxo ligand onto a water molecule from the bulk via a relay of two water molecules that was adjusted accordingly (see Scheme 1). Such a water relay was used instead of moving the proton just to a nearby solvent molecule in order to avoid immediate collapse of such a contact ion pair, yet to allow easy reprotonation through this relay (via the well-known Grotthus mechanism) in good time. With a hydronium ion nearby, the resulting $[UO_2(OH)_2(\kappa^1\text{-}O_2)(H_2O)]^{2-}$ complex should be rather unstable and rapid re-protonation was expected, either at the κ^1-peroxo site (restoring **2a**), or at one of the hydroxo ligands. It was the latter process that was observed: very quickly, within 0.2 ps, one of the OH ligands abstracted a proton from a nearby water molecule, affording $[UO_2(OH)(\kappa^1\text{-}O_2)(H_2O)_2]^-$, in which the κ^1-U-O-O moiety rapidly (within another 0.3 ps) collapsed to the κ^2-UO_2 ring affording **1a**. The simulation was stopped before the H_3O^+ and OH^- ions that were still present in the bulk could meet and neutralise each other.

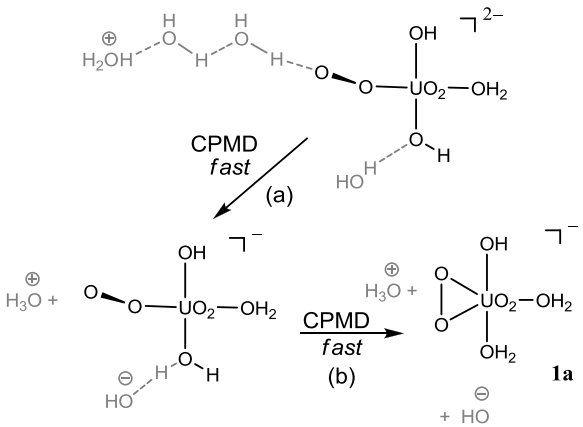

Scheme 1: CPMD simulations probing the fate of a κ^1-UO_2 complex in water (top): rapid proton transfer (a) and ring closure (b) restore peroxo complex **1a** (see text).

The spontaneous formation of **1a** rather than **2a** in this simulation may be taken as evidence for the stability of the former over the latter isomer. Hower, no firm conclusions can be drawn from such a singular event. We therefore decided to compute the relative free energy between these isomers, which are both stable in unconstrained CPMD runs, via constrained CPMD/PTI simulations.

We chose the difference coordinate $\Delta r = r(O^b\text{-}H^c) - r(O^a\text{-}H^c)$ for this purpose. In the last 2 ps of the unconstrained simulation of aqueous **1a**, Δr fluctuated around a value of ca. 1.91(29) Å. This value was taken as starting point for the constrained MD runs, and was successively decreased in steps of 0.32 Å, until a structure corresponding to **2a** was first obtained at a value of Δr = -0.97 Å. Between Δr = +0.31 Å and -0.33 Å, the mean constrained force changed from a large positive to a large negative value. To have a finer mesh in that region and to probe for possible hysteresis (a common plague of constrained MD simulations),[42] two additional points at Δr = -0.17 Å and +0.15 Å were sampled, retracing the path from the last point at Δr = -0.33 Å. The free-energy profile resulting from this procedure, along with representative snapshots along the path, is displayed in Figure 2.

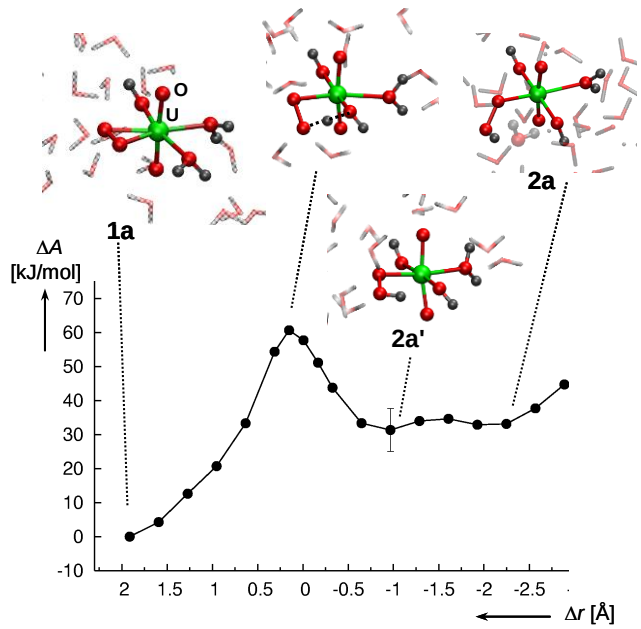

Figure 2: Free-energy profile for tautomerisation of aqueous uranyl-peroxo complexes from constrained CPMD/BLYP simulations, including representative snapshots from the trajectory (see Figure S2 in the ESI for an enlarged plot).

As the proton transfer from a water to the peroxo ligand proceeds starting from **1a**, the free energy increases, passing a barrier of $\Delta A^{\ddagger}$ = 60.7(±3.8) kJ/mol at Δr = +0.15 Å until an apparent minimum is reached at Δr = -0.97 Å, with ΔA = 31.3(±6.3) kJ/mol (**2a'** in Figure 2). As in our previous studies,[18] numerical uncertainties were estimated from standard deviations of the running averages of the mean constraint forces (over the last picosecond at each point,

multiplied with the integration width). Note that these uncertainties are just an indication of the numerical precision of the PTI technique, not of the intrinsic errors of our quantum-chemical model.

Tautomer **2a'** is characterised by an intramolecular H-bond donated from the dangling OOH moiety to the adjacent hydroxo ligand, a feature that is not retained in the gas-phase minima. When the path was continued in order to break this intramolecular H-bond, the OH moiety of the hydroperoxo ligand started to rotate out of the equatorial uranyl plane, and a water molecule from the bulk approached, accepting a H-bond from the OOH unit and donating one to the OH ligand (cf. **2a** in Figure 2; the additional water molecule is indicated as washed-out ball-and-stick representation, see also the blue arrow in the enlarged version in Figure S2).

With the chosen coordinate, little energetic discrimination between **2a'** and **2a** is apparent. At one point on this part of the path connecting the two, at Δr = -1.61 Å, this water molecule from the bulk suddenly acted as a relay for a proton transfer from the OOH moiety to the OH ligand (through bonds that are not involved in the constraint, see Figure S3 in the ESI for details). This process happened quickly (within 0.4 ps) under concomitant UO_2 ring closure, affording the reactant **1a**. In order to maintain the path, the simulation for this point (Δr = -1.61 Å) was thus repeated imposing an additional constraint on the OH bond of the water relay, which was fixed at its initial value of 0.98 Å. For the later points on the path beyond this Δr value, this additional constraint could be lifted without further occurrence of a similar, spontaneous proton transfer.

Again, the statistical significance of this singular event is limited, but it is another indication that **1a** is more stable than **2a** in aqueous solution. As such, it reinforces the conclusion from the PTI calculation that it is indeed **1a** that is preferred in water. A quantitative prediction for this preference is hampered by the fact that the BLYP functional used in the CPMD simulations affords slightly disparate results with the setups involved in our periodic and nonperiodic calculations (most likely due to the different pseudopotentials and, in particular basis sets), and that it also affords results that differ appreciably from the CCSD(T) benchmark (Table 1). A rough estimate can be given, however, as follows:

First, we probe the effect of using the larger basis by refining the point of highest constraint force (at Δr = +0.31 Å) with a higher cutoff. On going from 80 Ry to 100 Ry, this force increases slightly, from 0.01615(29) au to 0.01660(13) au (standard deviations σ over the last picosecond in parentheses). Even though both are essentially identical within 1σ, it is interesting to note that when the integral over the whole path is scaled by the resulting factor from this single point, the separation between **1a** and **2a'** increases from ΔA = 31.3 kJ/mol to 32.2 kJ/mol. In view of this small basis-set effect we did not recalculate the full path with this higher cutoff; instead we will use this "single-point" estimate.

Next, neglecting all enthalpic and entropic effects on the tautomeric equilibrium between **1a** and **2a** (which is a reasonable assumption, given that the B3LYP ΔE and ΔG values in Table 1 differ by less than 1 kJ/mol), solvation changes the relative stability of **2a** from -8.1 kJ/mol in the gas phase (CP-opt100 value in Table 1) to +32.2 kJ/mol in water (ΔA of **2a'** in Figure 2, scaled according to the preceding discussion), i.e. by ca. +40 kJ/mol at the BLYP level. Using this solvation free energy difference as an increment to correct the gas-phase energies in Table 1 (simply adding it to the ΔE_{rel} values in the rightmost column), affords estimates for the relative free energy of **2a** in water ranging from ca. +19kJ/mol or +22 kJ/mol (based on M06 or B3LYP energies, respectively) to +7 kJ/mol (based on the CCSD(T) energy). All these estimates agree with CPMD/BLYP that **1a** should be preferred in water. Only the less reliable HF and CCSD levels would predict **2a** to be more stable also in aqueous solution,

These estimates may not be the final answer, however, because **2a** may not be the actual species in solution. Uranyl complexes have a pronounced preference for the coordination number of five in the equatorial plane. If **2a** would attach an additional water molecule from the solution with a sufficiently large free binding energy, the resulting $[UO_2(OH)_2(\kappa^1\text{-}O_2H)(H_2O)_2]^-$ could still be present, if not prevalent, in solution. Apart from the nature of the spectator ligands, the affinity of four-coordinate uranyl complexes toward a fifth water ligand depends on the overall charge of the complex, and decreases with this charge. While dicationic complexes tend to bind water strongly, dianionic complexes may not bind a fifth ligand at all, examples being $[UO_2Cl_4]^{2-}$ [43] or, more relevant for the title compound, $[UO_2(OH)_4]^{2-}$.[44] For uranyl chloride complexes, high-energy X-ray scattering experiments suggest that the transition from five-to four-coordination occurs already at the neutral dichloride $UO_2Cl_2(H_2O)_n$ ($2+n$ = 4.3 on average), and that the monoanionic trichloride is four-coordinate, i.e. $[UO_2Cl_3(H_2O)]^-$,[45] in full agreement with predictions from DFT and CPMD/PTI simulations.[46]

An attempted optimisation of pristine $[UO_2(OH)_2(\kappa^1\text{-}O_2H)(H_2O)_2]^-$, starting from **2a**·$H_2O$ (Figure 1) with the "outer-sphere" water molecule pulled in toward U to create a roughly pentagonal bipyramidal environment of O atoms about the metal, resulted in spontaneous expulsion, apparently without barrier, of one of the water ligands (incidentally the one *trans* to the OOH ligand, affording another "4+1" isomer 11.8 kJ/mol higher than **2a**·H_2O at B3LYP/SDD). Even if cooperative polarisation in bulk water[47] would increase the affinity between **2a** and a fifth water ligand to a point that the latter would be bound in terms of ΔE or ΔH, it is unlikely that it would counterbalance the entropic penalty for such an associative process. In fact, when a CPMD simulation was started from the same five-coordinate structure for aqueous $[UO_2(OH)_2(\kappa^1\text{-}O_2H)(H_2O)_2]^-$ (after 1ps equilibration with all equatorial U-O bonds fixed), a water ligand (now the one *cis* to OOH) was expelled immediately into the bulk solution (with the U-O distance exceeding 3 Å within less that 0.1 ps).

To summarise this part, there is no evidence from experiment or computation that **2a** could be stabilised by binding a fifth water ligand to such an extent that it would be more stable than **1a**. We can thus predict the preference for the latter structure in aqueous solution with confidence.

It should be noted that the direct proton transfer followed in Figure 1 is not necessarily the true minimum energy path; it was chosen because it can be described by a simple reaction coordinate. Because there may be other channels for the same reaction with a lower barrier (in particular using water molecules from the bulk as relay, as discussed above for the spontaneous reverse event), the barrier in Figure 1 is just to be taken as an upper limit. As ΔA is a state function and thus, in principle, independent of the chosen path, the relative free energy between **1a** and **2a** should be reliable.

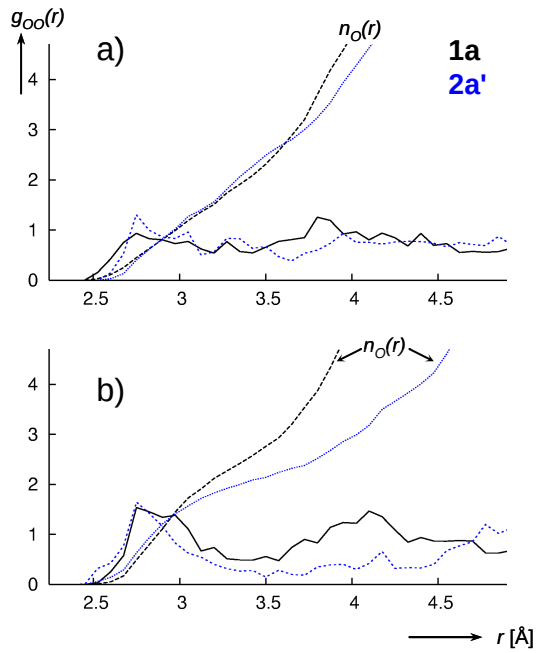

Figure 3: O(complex)-O(water) radial distribution functions $g_{OO}(r)$ for **1a** (black) and **2a'** (blue) on the constrained paths shown in Figure 1, evaluated between O atoms from the solution and a) the two peroxo O atoms ($O^{b,b'}$), or b) the single water or OH ligand (Oa).(n_O: integral $\rho\int g_{OO}(r)4\pi r^2 dr$ showing the mean number of O atoms in a sphere with radius r).

What is the reason for the large solvation effect that reverses the relative stability of **1a** and **2a** between gas phase and solution? It is difficult to pinpoint an obvious, clear-cut reason for this reversal from our simulations, but it appears that on going from **1a** to **2a'** on our path in Figure 1, peroxo and hydroperoxo moieties stay similarly well solvated (Figure 3a), whereas the water ligand in **1a** interacts more closely with the surrounding water than the OH ligand in **2a'** (Figure 3b - note the broader extent of the first maximum of g_{OO} between 2.5 Å and 3.5 Å and the concominant increase of the mean number of water molecules, n_O). As the water ligand in **1a** is converted into OH during formation of **2a'**, it thus forfeits part of its stabilisation from the solvent. The reinforcement of hydrogen bonds donated by metal-coordinated water ligands has been discussed recently.[48]

To study the solute-solvent interactions in more detail, hybrid QM/MM (quantum-mechanics/molecular-mechanics) simulations were performed for **1a** and **2a'**, starting from the last snapshots of the constrained CMPD trajectories (see SI for details) . Because all solvent molecules were included in the MM region, specific H-bond interactions may not be described with quantitative accuracy in these QM/MM simulations (also, proton transfer reactions involving the solvent are prevented). However, the solvent-solute interaction energies, $E_{QM\text{-}MM}$, are easily obtained and may inform qualitatively on the strength of solvation. When averaged over 15 ps of QM/MM-MD, the mean $E_{QM\text{-}MM}$ values (electrostatic part only, without van-der-Waals terms) were indeed more negative for **1a** (ca. -289 kJ/mol) than for **2a'** (-234 kJ/mol), confirming the better solvation of the former over the latter.

Table 2. Average relative energies and free energies (in kJ/mol), as well as dipole moments (in D) of the complexes in gaseous *vs* aqueous phase (in parentheses: standard deviations or estimated uncertanty).

Property	**1a**	**2a'**
Gas phase[a]		
Relative energy[b]	0.0	-30.5(228)
Dipole moment	11.8(6)	10.3(7)
In solution (PCM)[a,c]		
Relative energy[b]	0.0	37.4(152)
Relative free energy[d]	0.0	39.3(150)
Dipole moment	15.9(10)	13.7(10)
In solution (explicit solvent from CPMD)		
Relative free energy[e]	0.0	31.3(±6.3)
Dipole moment[f]	18.1(13)	16.3(12)

[a]Mean values over 50 snapshots taken from the constrained CPMD simulations in explicit water (over the last picosecond), in which only the complexes **1a** or **2a'** were retained (the solvent has been removed at each step). Single points at the BLYP/SDD/6-311+G** level. [b]SCF energies. [c]Employing the PCM model from Gaussian 03 with parameters of water and the same 50 snapshots have been used to compute the single points, at the same level. [d]SCF energies plus the sum of all non-electrostatic terms (see Table S1). [e]As obtained from the PTI calculation (see Figure 2). [f]Computed from Wannier Functions Centers (WFCs) on the same 50 snapshots, using the U atom as origin for the dipole moment.

Further analysis of the QM region in these QM/MM simulation revealed that **1a** had a much larger mean dipole moment (ca. 16 D) than **2a'** (ca. 8 D).[49] When the dipole moments of the solutes were evaluated for the purely quantmum-mechanical CPMD simulations (through analysis of the Wannier function centers for a number of snapshots from the last picosecond of the constrained MD runs, see SI

Table 3. Optimised or mean simulated bond distances in **1a** (in Å, for labeling scheme see Chart 2).

Level[a]	U=O[b]	U-O^b	U-O$^{b'}$	U-O^{a}H$_2$	U-OH$_2$	U-OH	O^b-O$^{b'}$
CP-opt(g)	1.873	2.248	2.178	2.773	2.832	2.333	1.478
BLYP(g)	1.873	2.253	2.214	2.805	2.845	2.311	1.457
B3LYP(g)	1.827	2.222	2.182	2.721	2.782	2.307	1.440
B3LYP(PCM)	1.836	2.241	2.227	2.572	2.618	2.223	1.459
CPMD(aq)	1.90(4)	2.27(8)	2.24(7)	2.69(16)	2.53(9)	2.26(8)	1.49(2)

[a]CPMD(aq): mean values during the last 2 ps of unconstrained MD (BLYP level, standard deviation in parentheses) in water; BLYP, B3LYP: optimised parameters using the respective functional (SDD basis).
[b]Mean value for the bonds to the terminal uranyl O atoms.

for details), the resulting values were more similar, but still slightly higher for **1a** (ca. 18 D) than for **2a**' (ca. 16 D). Thus,in addition to specific solute-solvent interactions, bulk solvation is also indicated to contribute to the stabilisation of **1a** in water. When PCM calculation are performed for the bare solutes taken from these snapshots, similar results are obtained in terms of polarised solute-solvent energies and dipole moments (see Tables 2 and S1).

Because of the large fluctuations of energies and dipole moments over these snapshots (see standard deviations in parentheses), the quantitative results in Table 2 should not be overinterpreted, but qualitatively they confirm the conclusions from CPMD, namely that **1a** is disfavored in the gas phase, but more stable in water, where it is better solvated and has a higher dipole moment than **2a**. When averaged over the CPMD snapshots, the simple PCM energies favor **1a** as well, in line with the static optimisations in a continuum (Table 1). Explicit and bulk solvation thus appear to be closely linked, and the structures arising from the former are important for the latter.

To conclude this section, optimised and MD-simulated structural parameters of **1a** are collected in Table 3 for further reference. Whereas the U-O$^{b,b'}$ bonds involving the κ^2-peroxo unit expand slighly upon solvation (compare CP-opt and CPMD(aq) data in Table 3), U-OH$_2$ and U-OH bonds contract noticeably, in particular that involving the water ligand trans to the peroxo unit (by ca. -0.3 Å), but also the one adjacent to it (by -0.08 Å, cf. U-O^{a}H$_2$ values). Similar trends are seen upon optimisation in the continuum (compare B3LYP(g) and B3LYP(PCM) data in Table 3). In contrast, the corresponding U-O^{a}H bond in **2a** does not experience such a contraction upon solvation: in fact, upon going from CP-opt toCPMD(aq) this distance increases slightly, by ca. +0.02 Å (data not shown), in qualitative accord with the arguments on the differential solvation of OH and water ligands discussed above.

4 Conclusions

In summary, we have used static DFT and ab initio calculations, as well as DFT-based MD simulations, to complement recent experimental speciation studies of uranyl peroxo complexes. Focusing on a possible tautomeric equlibrium between complexes with a κ^2-UO$_2$ metallacycle (**1a**) and a κ^1-UOOH moiety (**2a**), it turns out that the latter is indicated to be significantly more stable than the former in the gas phase. According to optimisations with a simple polarisable continuum model and to constrained CPMD/PTI simulations, however, this relative order of stability is reversed in aqueous solution, where **1a** is preferred, most likely due to differential solvation of the ionic (peroxo, hydroxo) vs. neutral ligands (water). After correction for intrinsic deficiencies of the BLYP functional used in these MD simulations (by calibrating against gas-phase energies obtained at hybrid DFT and CCSD(T) level), the hydroperoxo tautomer **2a** is estimated to be between ca. +7 kJ/mol to +22 kJ/mol higher in (free) energy than **1a**. This result can be taken as strong evidence that it is indeed the latter species that is present in the speciation equilibria.

When only the general constitution of uranyl complexes can be determined experimentally, but not their precise structure, this missing information can be obtained from quantum-chemical calculations. As the present study demonstrates once more, proper description of solvation effects is of the essence if ionic (and/or polar) substrates are immersed in a polar, protic solvent.

Acknowledgement: This work was supported by the EaStCHEM School of Chemistry via the EaStCHEM Research Computing facility and a local Opteron PC cluster maintained by Dr. H. Früchtl. N.S. thanks the UJF and the CNRS for financial support and the CECIC (project: liqsim) for computer resources. NWChem calculations made use of the facilities of HECToR, the U.K. national high-performance computing service, which is provided by UoE HPCx Ltd. at the University of Edinburgh, Cray Inc., and NAG Ltd. and funded by the Office of Science and Technology through EPSRC's High End Computing Programme.

Notes and references

[a] *EaStCHEM School of Chemistry, North Haugh, University of St. Andrews, St. Andrews, Fife KY16 9ST, UK, E-mail: buehl@st-andrews.ac.uk*
[b]*Département de Chimie Moléculaire, UMR-5250, ICMG FR-2607, CNRS, Université Joseph Fourier Grenoble I, 301 rue de la Chimie, BP 53, 38041 Grenoble Cedex 9, France.*
[c]*UMR 7177 CNRS, Laboratoire MSM, Institut de Chimie, 1 rue Blaise Pascal, 67000 Strasbourg, France.*

† Electronic Supplementary Information (ESI) available: Additional computational details and references (including full citations for

reference 34), additional graphical material and optimised coordinates of complexes **1a** and **2a**. See DOI: 10.1039/xxxx/

1 (a) H. Christensen, T. Sunder, *Nucl.Technol*., 2000, **131**, 102–123; (b) C. Corbel, G. Sattonnay, S. Guilbert, F. Garrido, M. F. Barthe, C. Jegou, *J. Nucl. Mater*., 2006, **348**, 1-17.
2 E.g. after the Fukushima accident: C. R. Armstrong, M. Nyman, T. Shvareva, G. E. Sigmon, P. C. Burns, A. Navrotsky, *Proc. Nat. Acad. Sci*., 2012, **109**, 1874–1877.
3 P. C. Burns, K. A. Hughes, *Am. Mineral*., 2003, **88**, 1165 – 1168.
4 See also the bibliography in: C. Mallon, A. Walshe, R. J. Forster, T. E. Keyes, R. J. Baker, *Inorg. Chem*., 2012, **51**, 8509−8515.
5 Review: J. Qiu, P. C. Burns, *Chem. Rev*. 2013, **13**, 1097-1120.
6 For a recent review see e.g.: R. J. Baker, *Chem. Eur. J*., 2012, **18**, 16258-16271.
7 For a recent study of uranium peroxide precipitation see: K. W. Kim, J. T. Hyun, K. Y. Lee, E. H. Lee, K. W. Lee, K. C. Song, J. K. Moon, *J. Hazard. Mater*., 2011, **193**, 52-58.
8 P. L. Zanonato, P. Di Bernardo, I. Grenthe, *Dalton. Trans*. 2012, **41**, 3380-3386.
9 P. L. Zanonato, P. Di Bernardo, Z. Szabo, I. Grenthe, *Dalton. Trans*. 2012, **41**, 11635-11641.
10 A. Martinez-Torrents, S. Meca, N. Baumann, V. Marti, J. Gimenez, J. de Pablo, I. Casas, *Polyhedron* 2013, **55**, 92-101.
11 K. W. Kim, E. C. Jung, K. Y. Lee, H. R. Cho, E. H. Lee, D. Y. Chung, *J. Phys. Chem. A*, 2012, **116**, 12024-12031.
12 We note that although well-characterised metal hydroperoxo complexes are rare, there are several examples of such species (a search for M-O-O-H fragments in the Cambridge Structure Database returns 12 hits); selected examples comprise V(V) or Pd(II) complexes: (a) M. Šimuneková, J. Šimunek, J. Chrappová, P. Schwendt, Z. Žák, F. Pavelčík, *Inorg. Chem. Commun*., 2012, **24**, 125-128; (b) X. Cai,, S. Majumdar, G. C. Fortman, C. S. J. Cazin, A. M. Z. Slawin, C. Lhermitte, R. Prabhakar, M. E. Germain,, T. Palluccio,, S. P. Nolan,, E. V. Rybak-Akimova, M. Temprado, B. Captain, Carl D. Hoff, *J. Am. Chem. Soc.*, 2011, **133**, 1290-1293.
13 Fore some selected reviews see: (a) D. Wang, W. F. van Gunsteren, Z. Chai, *Coord. Chem. Rev.*, 2012, **41**, 5836-5865; (b) G. A. Shamov, *Acc. Chem. Res*., 2010, **43**, 19-29; (c) R. G. Denning, *J. Phys. Chem. A*, 2007, **111**, 4125-4143; (d) Z. Szabó, T. Toraishi, V. Vallet, I. Grenthe, *Coord. Chem. Rev.*, 2006, **250**, 784-815; (e) N. Kaltsoyannis, P. J. Hay, J. Li, J. P. Blaudeau, B. E. Bursten, in: *The Chemistry of the Actinide and Transactinide Elements*, 3rd ed.; Morss, L. R., Edelstein, N. M., Fuger, J., Katz, J. J., Eds.; Springer: Dordrecht, The Netherlands, 2006; Vol. 3, pp 1893-2012.
14 S. O. Odoh, G. Schreckenbach, *Inorg. Chem*., 2013, **52**, 5590-5602.
15 V. Vallet, U. Wahlgren, I. Grenthe, *J. Phys. Chem. A*, 2012, **116**, 12373-12380.
16 P. F. Weck, E. Kim, C. F. Jove-Colon, D. C. Sassani, *Dalton Trans*., 2012, **41**, 9748-9752.
17 E.g.: (a) P. Wåhlin, B. Schimmelpfennig, U. Wahlgren, I. Grenthe, V. Vallet, Theor. Chem. Acct., 2009, 124, 377-384; (b) K. E. Gutowski, D. A. Dixon, *J. Chem. Phys. A*, 2006, **110**, 8840-8856; (c) V. Vallet, H. Moll, U. Wahlgren, Z. Szabo, I. Grenthe, *Inorg. Chem*., 2003, **42**, 1982-1993.
18 Review: M. Bühl, G. Wipff, *ChemPhysChem*, 2011, **12**, 3095-3105.
19 For more recent applications of this technique see: (a) M. Bühl, I. Grenthe, *Dalton Trans.*, 2011, **40**, 11192-11199; (b) M. Bühl, N. Sieffert, A. Chaumont, G. Wipff, *Inorg. Chem.*, 2012, **51**, 1943-1952.
20 For other first-principles MD simulations of uranyl hydrate see: (a) R. Spezia, B. Siboulet, S. Abadie, R. Vuilleumier, P. Vitorge, *J. Phys. Chem. B*, 2011, **115**, 3560–3570; (b) R. J. Frick, T. S. HoferA. B. Pribil, B. R. Randolf, B. M. Rode, *J. Phys. Chem. A*, 2009, **113**, 12496–12503 (c) P. Nichols, E. J. Bylaska, G. K. Schenter, W. de Jong, *J. Chem. Phys.*, 2008, **128**, 124507. (d) D. Hagberg, G. Karlström, B. O. Roos, L. Gagliardi, *J. Am. Chem. Soc*., 2005, **127**, 14250-14256.
21. R. Car, M. Parrinello, *Phys. Rev. Lett*., 1985, **55**, 2471-2474.
22 (a) A. D. Becke, *Phys. Rev. A*, 1988, **38**, 3098-3100; (b) C. Lee, W. Yang, R. G. Parr, *Phys. Rev. B*, 1988, **37**, 785-789.
23 M. Bühl, R. Diss, G. Wipff, *J. Am. Chem. Soc*., 2005, **127**, 13506-13507.
24 The initial CPMD/BLYP simulations in the Parrinello group have afforded good descriptions of liquid water, see for instance: (a) M. Sprik, J. Hutter, M. Parrinello, *J. Chem. Phys*., 1996, **105**, 1142-1152, although potential shortcomings of this functional are now better appreciated, see: (b) J. VandeVondele, F. Mohamed, M. Krack, J. Hutter, M. Sprik, M. Parrinello, *J. Chem. Phys.*, 2005, **122**, 014515 and references cited therein.
25 CPMD Versions 3.7.0 and 3.13.1, Copyright IBM Corp. 1990-2008, Copyright MPI für Festkörperforschung Stuttgart 1997 - 2001.
26 A. D. Becke *J. Chem. Phys.* 1993, **98**, 5648; C. Lee, W. Yang, R. G. Parr, *Phys. Rev. B* 1988, **37**, 785.
27 (a) W. Küchle, M. Dolg, H. Stoll, H. Preuss,*J. Chem. Phys*., 1994, **100**, 7535-7542.
28 This small-core ECP has been shown to reproduce all-electron scalar relativistic results very well, see: S. O. Odoh, G. Schreckenbach, *J. Phys. Chem. A*, 2010, **114**, 1957-1963.
29 R. Krishnan, J. S. Binkley, R. Seeger, J. A. Pople, *J. Chem. Phys*., 1980, **72**, 650-654.
30 B3LYP geometries were employed because for uranyl hydrate, they have performed very well in single-point energy calculations using migh-level multireference methods: F. P. Rotzinger, *Chem. Eur. J*., 2007, **13**, 800 – 811
31 (a) T. H. Dunning, Jr., *J. Chem. Phys*. 1989, **90**, 1007-1023; (b) R. A. Kendall, T. H. Dunning, Jr., R. A. Harrison, *J. Chem. Phys*. 1992, **96**, 6769-6806.
32 Y. Zhao, D. G, Truhlar, *Theor. Chem. Acct*. 2008, **120**, 215-241.
33 as implemented in Gaussian 09: (a) V. Barone, M. Cossi, J. Tomasi, *J. Comput. Chem.*, 1998, **19**, 404-417; (b) M. Cossi, G. Scalmani, N. Rega, V. Barone, *J. Chem. Phys*., 2002, **117**, 43-54. (c) M. Cossi, O. Crescenzi, *J. Chem. Phys.*, 2003, **19**, 8863-8872; review: (d) J. Tomasi, B. Mennucci, R. Cammi, *Chem. Rev*., 2005, **105**, 2999-3093.
34 (a) M. J. Frisch, et al., Gaussian 03, Revision E.01, Gaussian, Inc., Wallingford CT, 2004; (b) M. J. Frisch, et al., Gaussian 09, Revision A.02, Gaussian, Inc., Wallingford CT, 2009 (see SI for full references).
35 M. Valiev, E. J. Bylaska, N. Govind, K. Kowalski, T. P. Straatsma, H. J. J. van Dam, D. Wang, J. Nieplocha, E. Apra, T. L. Windus, W. A. de Jong, *Comput. Phys. Commun*. 2010, **181**, 1477-1489 (Version 6.1.1).
36 S. Grimme, J. Antony, S. Ehrlich, H. Krieg, *J. Chem. Phys*, 2010, **132**, 154104.
37 This level has also been successfully used to rationalise the barrier involved in the uranyl "yl-exchange": M. Bühl, G. Schreckenbach, *Inorg. Chem*. 2010, **49**, 3821-3827.
38 Based on results for the water-exchange barriers in uranyl hydrate, see: J. P. Austin, N. A. Burton, I. H. Hillier, M. Sundararajan, M. A. Vincent, *Phys. Chem. Chem. Phys*., 2009, **11**, 1143-1145.
39 P. Wåhlin, C. Danilo, V. Vallet, F. Réal, J.-P. Flament, U. Wahlgren, *J. Chem. Theor. Comput*., 2008, **4**, 569–577.
40 Due to program limitations, the so-called T_1-diagnostic (J. T. Lee, P. R. Taylor. *Int. J. Quantum Chem. Symp*. 1989, **23**, 199-207) could not be printed after the CCSD calculations with NWChem. This property is an indication of possible shortcomings of the Hartree-Fock single-reference wave function. With a smaller basis set (no g-functions on U, aug-cc-pVDZ on O, cc-pVDZ on H), this diagnostic could be computed with Gaussian 03, where it amounted to 0.026 and 0.022 for **1a** and **2a**, respectively (with a similar relative energy of the latter, -55 kJ/mol, as the CCSD/SDD+ energy in Table 1). These numbers are somewhat above the commonly used threshold for the need for a multi-determinantal ansatz (0.02), but similar to those computed for uranyl hydrate (reference 39) or for *cis*- and *trans*-uranyl complexes involved in the yl-exchange (reference 37). Note that transition-metal complexes with T_1-values up to 0.05 have been classified as single-reference cases (W. Jiang, N. J. DeYonker, A. K. Wilson, *J. Chem. Theor. Comput*., 2012, **8**, 460–468).
41 See for instance: F. R. Rotzinger, *J. Phys. Chem. B*, 2005, **109**, 1510-1527.

42 See e.g.: A. E. Mark, C. P. van Helden, P. E. Smith, L. H. M. Janssen, W. F. van Gunsteren, *J. Am. Chem. Soc.*, 1994, **116**, 6293-6302.
43 L. di Spio, E. Tondello, G. Pellizzi, G. Ingletto, A. Montenero, *Cryst. Struct. Commun*. 1974, **3**, 297-300.
44 (a) D. L. Clark, S. D. Conradson, R. J. Donohoe, D. W. Keogh, D. E. Morris, P. D. Palmer, R. D. Rogers, C. D. Tait, *Inorg. Chem*. 1999, **38**, 1456-1466; (b) U. Wahlgren, H. Moll, I. Grenthe, B. Schimmelpfennig, L. Maron, V. Vallet, O. Gropen, *J. Phys. Chem. A* 1999, **103**, 8257-8264.
45 L. Soderholm, S. Skanthakumar, R. E. Wilson, *J. Phys. Chem. A* 2011, **115**, 4959-4967.
46 M. Bühl, N. Sieffert, V. Golubnychiy, G. Wipff, *J. Phys. Chem. A* 2008, **112**, 2428-2436.
47 M. Bühl, N. Sieffert, A. Chaumont, G. Wipff, *Inorg. Chem.*, 2011, **50**, 299–308.
48 J. M. Andric, G. V. Janjic, D. B. Ninkovic, S. D. Zaric, *Phys. Chem. Chem. Phys.* 2012, **14**, 10896–10898.
49 We used the U atom as origin for evaluating the dipole moment; for discussion of ab initio MD-derived dipole moments of ions, see e.g.: M. Brehm, H. Weber, A. S. Pensado, A. Stark, B. Kirchner, *Phys. Chem. Chem. Phys*., 2012, **14**, 5030–5044.